Automating the assessment of orbit predictions and estimations for building and maintaining a new catalogue

Michael Lachut*, **James Bennett**
EOS Space Systems Pty Ltd, Queanbeyan NSW Australia
Space Environment Research Centre, Mount Stromlo ACT Australia
David Kooymans
EOS Space Systems Pty Ltd, Queanbeyan NSW Australia

Abstract

One of the primary aims of the Space Environment Research Centre (SERC) is to build and maintain its own catalogue of objects in near-Earth orbits. This will provide accurate ephemeris data for object acquisition in both passive and active tracking, covariance matrices for sensor schedule tasking and observation correlation, state and uncertainty propagation for conjunction assessments, and help facilitate the remote maneuver of debris using high powered lasers delivered from ground stations, which is the primary objective of SERC. The catalogue comprises objects which pose a threat of colliding with Optus satellites identified in conjunction assessments, potential candidates for the laser maneuver, and other objects of interest for ongoing research including Envisat, Topex, small cubesats, and HAMR debris.

In this paper, we will present methods to automate the assessment of orbit predictions and estimations to maintain and build a new catalogue of space assets and debris. The process begins by running an orbit determination seeded by parameters stored in a catalogue and/or publicly available. The characteristics of an object of interest determined during the orbit estimation, such as the ballistic coefficient or radiation coefficient, are assessed as to whether they are within physical limits and are also compared against historic estimated values to test validity. In the event of a new object where no historic data is available, ballistic/radiation coefficients are stored and not used until a sufficient number is available to achieve statistical confidence in the stored values. Alternatively, a ballistic coefficient estimation method for low objects and an equivalent method for higher orbits can be used.

The observation residuals generated from the orbit determination (OD) process are assessed as to whether they are within a given threshold based on the nominal noise of each sensor within our network. Comparisons of observations with highly accurate external ephemeris data from the International Laser Ranging Service (ILRS) are presented to show the level of sensor noise. If the RMS of an observation arc is above a threshold, which is set based on the observation weighting factor, the pass is automatically weighted weaker thus increasing the threshold for that pass. At this point, the OD process runs iteratively until all observation arcs stay within their respective thresholds. This ensures that outliers are tagged and kept quarantined in the catalog.

The next step is to assess the prediction accuracy of the generated ephemeris data. The generated state from the OD process is propagated backwards and compared against observation arcs before the OD starting epoch. Regression models based on historic data from the catalog are used to set the threshold limits for predictions lengths dictated by varies orbital regimes. If a pass falls outside the predication threshold, the ephemeris data is quarantined and assessed manually for accuracy and reliability. Results are demonstrated here for the different orbital regimes considered.

1. INTRODUCTION

One of the primary objectives of the Space Environment Research Centre (SERC) is to maneuver a near earth debris object to avoid a collision using ground based lasers. This requires accurate orbit estimations and predictions to ensure the object is not perturbed into a less favorable orbit which in the worst case scenario could potentially cause a collision with an active near earth satellite. A high powered continuous wave (CW) laser coupled with adaptive optics [1] will be used to apply photon pressure onto the object using the 1.8 meter telescope at EOS Space Systems' Debris Tracking Station located at Mt. Stromlo in Canberra Australia. The Mt. Stromlo site consists of a 1.8 meter telescope built by EOS and a 0.7 meter Planewave telescope. The Learmonth site contains two 1 meter telescopes

*Email: michaellachut@serc.org.au

designed and built by EOS as well as two 0.7 meter Planewave telescopes. The Mt. Stromlo telescopes are used mainly for research and development whereas the Learmonth site is commercial and fully operational.

Another aim of SERC is to provide a conjunction and threat warning service (CATW) which consists of building and maintaining a catalog of highly accurate states and covariances in order to perform error state propagation[1], non-spherical object characterization [2], high performance orbital propagation to perform time of closest approach conjunction assessments [3] and collision probabilities[2]. The goal of this paper is to discuss the process that builds and maintains a new catalog of objects by storing results from orbit determination and prediction processes. The methods involved in checking the unknown force parameters, residuals between observation tracklets and states during the orbit determination process as well as the quality of the propagated states are discussed.

2. METHOD

In this section, we outline the methodology used in the orbit determination (OD) process; an overview is provided in Fig. 1(a). A batch least-squares (BLS) approach has been implemented which requires a predefined OD span set by requiring at least three observation tracklets spread over at least 3 days and up to a maximum span of 10 days. These are the base requirements for a reliable orbit solution from passive-only data. Initially the tracklets are weighted by default values based on the nominal sensor noise of the sensor network. We provide examples of the network accuracy in Sec. 3. The default telescope tracking configuration is to collect observations by tracking the objects rather than the star field; however they can also perform stare and chase for new objects. After the observations have been collected they are then correlated to objects by ensuring they fall within a probability gate defined by propagating the error state covariances from our OD processes. In the event of no a priori state information, an OD process fitting pseudo observations generated by propagating TLEs using SGP4 can be used. If both of these methods cannot be performed then the correlation process is carried out by propagating a single TLE using SGP4 and a linear propagation of a nominal error covariance. If sufficient stars fall within the field of view, the tracklets are astrometrically corrected.

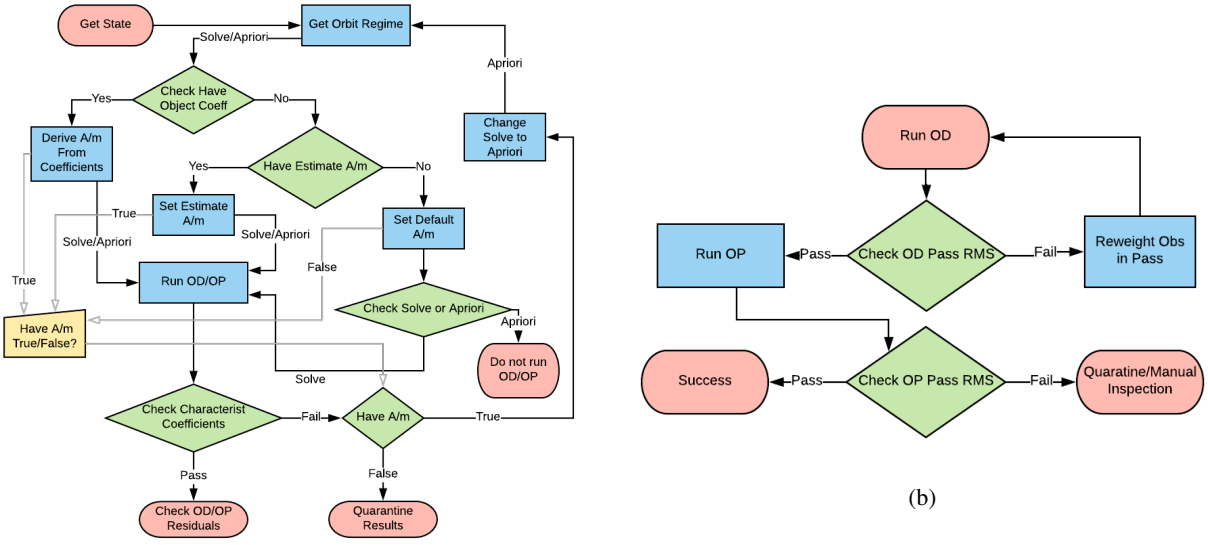

Figure 1. (a) Process to check for practical force coefficients such as the ballistic or SRP coefficient. (b) Process to check residuals during orbit determination and prediction.

Once sufficient observations become available, an OD process is triggered and the procedure begins by loading all of the standard libraries including EGM 96 Earth gravity and tides models, NRLMSIS-00 density model, solar radiation flux, JPL planetary ephemeris data and General relativity models into memory. Next, an initial state vector

[1]Further details are presented in a companion paper by Sven Flegel "Normality in State Uncertainties from Orbit Determination Results fitting Optical Measurements"

[2]An overview is given in a companion-paper by Bennett, Lachut et al., "Progress in a new conjunction and threat warning service for Space Situational Awareness and an analysis of a 2016 hitomi breakup event is given in Ref. [4]"

is set and then since a cannon-ball model is assumed the area-to-mass ratio (A/m) is estimated using the ballistic or solar radiation coefficient with default values for $C_D = 2.2$ and $C_R = 1.1$. In order to know what force models to use, the orbital regime of an object needs to be determined. Table 1 provides the definitions of the different orbit regimes used as well as the force models used in each one. The automation procedure can then check if a historic ballistic and/or solar radiation are stored in the database. If there are sufficient estimates, the average value is used to derive the initial area-to-mass ratio, which seeds the OD process. If not, the process checks whether an estimate of the A/m can be derived from using the Ballistic Coefficient Estimate Method [5] or a similar method in the case of SRP. Alternative approaches for operational or defunct satellites may include using their schematics (where available) or obtaining object characteristics using automated web scraping tools [6]. When all of the prior cases are unsuccessful a default value for $A/m = 0.001$ is used with the same aforementioned values of the force coefficients, C_D and C_R.

Table 1. Orbital regime definitions. The parameters $h_{\text{GEO}} = 35785.9$ km, $a_{\text{GEO}} = 42164$ km and $r_\oplus = 6378.137$ km. The semi-major axis is $a = \frac{h_p+h_a+2r_\oplus}{2}$, where h_p and h_a are the perigee and apogee altitudes, respectively. The eccentricity, e, is defined as: $e = \frac{h_p-h_a}{h_p+h_a+2r_\oplus}$. It is considered small if $e < 0.25$, and large if above. The inclination, i, is considered equatorial if $i < 1$, with the usual definition for prograde and retrograde orbits. The orbital period is given by P.

Orbital Regimes	h_p (km), h_a (km) or P (min)	Eccentricity e	Inclination i	Force Model
Lower LEO	$0 \text{ km} < \frac{h_p+h_a}{2} < 600$ km			Drag
Med LEO	$600 \text{ km} < \frac{h_p+h_a}{2} < 1000$ km			Drag, SRP
High LEO	$1000 \text{ km} < \frac{h_p+h_a}{2} < 2000$ km			SRP
MEO	$\frac{h_p+h_a}{2} > 2000$ km and $a < 0.9\, a_{\text{GEO}}$	Small		SRP
LHEO[3]	$h_p < 1000$ km, $h_a < h_{\text{GEO}} - 200$ km not Molynia	Large		Drag, SRP
HEO	$h_p > 1000$ km, $h_a < h_{\text{GEO}} - 200$ km not Molynia	Large		SRP
Molynia	$690 \text{ min} < P < 750$ min		$60^\circ \leq i \leq 68^\circ$	SRP
LGTO[3]	$h_p < 1000$ km, $h_a > h_{\text{GEO}} - 200$ km	Large		Drag, SRP
GTO	$h_p > 1000$ km, $h_a > h_{\text{GEO}} - 200$ km	Large		SRP
GEO	$h_p > h_{\text{GEO}} - 200$ km, $h_a < h_{\text{GEO}} + 200$ km	Small		SRP
EGO[4]	$0.9\, a_{\text{GEO}} < a < 1.1\, a_{\text{GEO}}$ not GEO	Small		SRP
Super GEO	$h_p > h_{\text{GEO}} + 200$ km	Small		SRP

At this point a global iteration process begins where either C_D and/or C_R are estimated. In order to update the initial state the observation tracklets are used to form the BLS normal equations [8] which are solved for the state at the initial epoch. This subprocess (within the current global iteration) is repeated iteratively until convergence occurs – if the process diverges the OD results are quarantined and post analyzed manually. Importantly, in the event that the initial estimated A/m is significantly incorrect, its error will be absorbed into the ballistic or solar radiation coefficients. For this reason, the process which solves the normal equations is run again where A/m is re-adjusted so that the ballistic and SRP coefficient are reset back to $C_D = 2.2$ and $C_R = 1.1$. It usually takes about 2-3 iterations for this process to converge. Once that has happened the ballistic and/or SRP coefficients are checked to be within their usual physical bounds. When this check fails the current global iteration is restarted with an a priori A/m, but only when the default $A/m = 0.001$ is not set, otherwise the process stops and results go into quarantine. If the force coefficient check passes then the procedure moves on to assess the RMS of the residuals between observation tracklets with respect to the estimated state (converted to observation space).

The next phase of the orbit determination and prediction assessment now commences; see Fig. 1(b). If the RMS of all the residuals during the OD span fall within their respective limits (in the initial iteration these would simply be those defined by the nominal sensor noise), the process moves onto the next stage which assesses the validity of the state orbit prediction (OP). If at least one of the tracklet RMS residuals exceed the threshold, the weighting for those tracklets is updated to the current RMS of its residual and becomes the new threshold, but only for that specific tracklet. The OD process is then repeated iteratively until all residual RMS values fall within their respective thresholds. This allows for the re-weighted tracklet to be tagged with a higher weighting and warn future processes that it should be

[3]The "L" in front of the orbit regime is an in-house term we use at SERC and EOS to indicate that an object comes deep enough into the atmosphere where we would apply atmospheric drag

[4]This orbit regime was adopted from the ESA Classification of Geosynchronous Objects [7]

weighted weaker and treated with caution. While this does not attempt to correct the tracklet, it allows the overall OD process to re-adjust the covariance by accounting for higher uncertainty in the measurement.

Once the OD assessment is complete and successful the OP assessment then checks the propagated state (in observation space) against observation tracklets before the initial epoch of the OD span that have been previously validated. Unlike the thresholds used during the OD span, the threshold during the OP span increases as a function of time, i.e., the further the state is propagated backwards the larger the drift in the back predicted state. Importantly, different orbit regimes can exhibit different levels of drift. In Section 3, we provide results which demonstrate the level of drift in the back propagated state after one week.

3. RESULTS AND DISCUSSION

In this section, we begin by presenting results for the nominal sensor noise of the Learmonth site. While EOS currently has another site at Mt.Stromlo as part of its network, recently the 1.8 meter telescope was undergoing upgrades and the 0.7 meter Planewave system was assigned for high frame-rate light curve studies[5]. As such, only the sensors at Learmonth were available to provide observations for recent orbit determination and predication results presented here. In Fig. (2), residuals for mount encoder measurements and astrometrically corrected observations with respect to ephemeris data (converted to observation space) publicly available from the ILRS are shown for all telescopes at Learmonth and for several orbit regimes. Figure (2(a)), shows the lowest residuals for the encoder

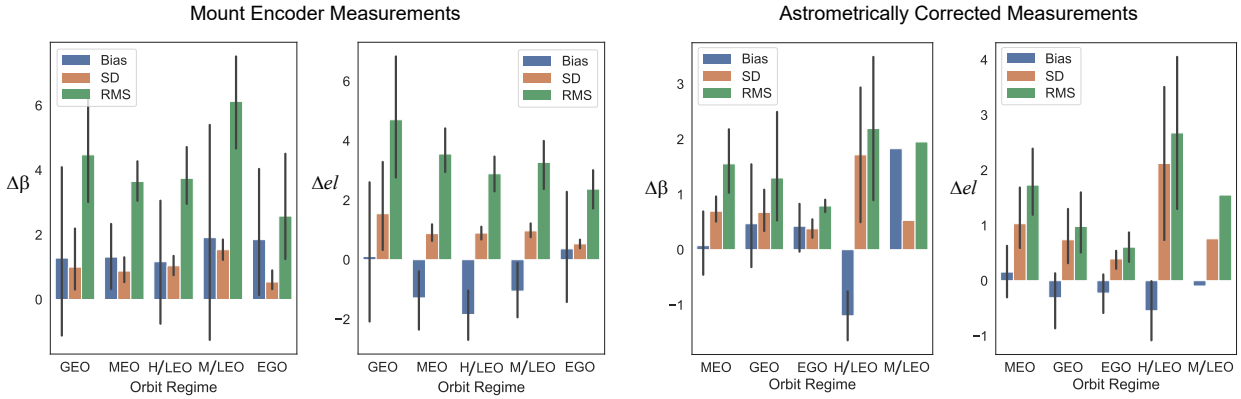

Figure 2. (a) Residuals between mount encoder measurements from all sensors at Learmonth compared to ILRS ephemeris data. (b) Residuals between astrometrically corrected measurements from all Sensors at Learmonth compared to ILRS ephemeris data.

measurements for objects in EGO orbits with a delta azimuth $\Delta\beta$ and elevation Δel RMS residual just above $2''$; the worst appears in the medium LEO orbits, which is to be expected, with a median $\Delta\beta \approx 6''$ and median $\Delta el \approx 5''$. In all cases the bias and standard deviation in the residuals does not exceed $2''$. In order to explain the slightly higher then expected mount encoder RMS values experienced for GEO targets, it is important to note that the Planewave telescopes are primarily tasked to track higher earth objects and as such do not require the same mount stability. These Planewave systems do not have the same encoder accuracy of the 1 meter systems which are designed to accurately track lower orbiting objects. In addition, and perhaps more importantly, the GEO targets considered here are actively maneuvering on a regular basis. As such, the accuracy is only as good as the quality of the prediction provided, which can vary by several arc-seconds especially near maneuvers.

The corresponding astrometrically corrected data is provided in Fig. (2(b)). Immediately, we can see that there is an overall reduction in the residuals by a factor of about 2-3, with the worst median RMS of $\Delta el \approx 2.5''$. The lowest RMS values are again for the EGO orbits [$(\Delta\beta, \Delta el) < 1''$ RMS] with the second best being GEO [$(\Delta\beta, \Delta el) \approx 1''$ RMS] then followed by MEO [$(\Delta\beta, \Delta el) < 2''$]. This makes sense since the Planewave telescopes now take advantage of their wide field of view which are able to collect a lot more stars to be used for astrometric correction. Interestingly, the medium LEO objects have a lower RMS than the high LEO, however, differences in the number of tracklets collected

[5]Results from analyzing these measurements are presented in a companion-paper by Daniel Kucharski, "High Sampling Rate Photometry of Spinning Satellites for Nano-Perturbation Detection", presentation ID 18AB00183

in each regime may explain this difference. While the astrometrically corrected data in the worst case was of the order of $\sim 2''$, work is currently underway on the underlying algorithms to approach sub arc-second level accuracy for LEO orbits on all systems.

A similar figure is provided in Fig. 3, except now we use the ephemeris data generated during our own OD processes. Since we do not currently have the capability to fit orbits of maneuvering objects in automated operations, here we only consider non-operational satellites and debris. The automation of the OD process fitting maneuvering objects is underway. The OD procedure used passive observation data fused with weakly weighted pseudo measurements generated from propagating TLE using SGP4 to enhance object observability. The residuals for the mount encoder data resulting from in-house ephemeris data are of similar order to what was observed in Fig. 2(a), only now the GEO orbits tend to give lower residuals than the EGO and MEO orbits. Interestingly, the Medium LEO residuals are lower then the Higher LEO targets. This can be explained due to the one meter systems mainly tracking the medium LEO targets whereas the Higher LEO targets consist of a mixture of tracking between all systems, i.e., the 1 meter systems have been specifically designed by EOS for accurate tracking in LEO. Nevertheless, the overall mount accuracy in high LEO orbits has not been hindered significantly. Figure 3(b) shows the astrometrically corrected residuals are below $2''$ for GEO, EGO and MEO orbits, with higher residuals for the low earth objects which is to be expected.

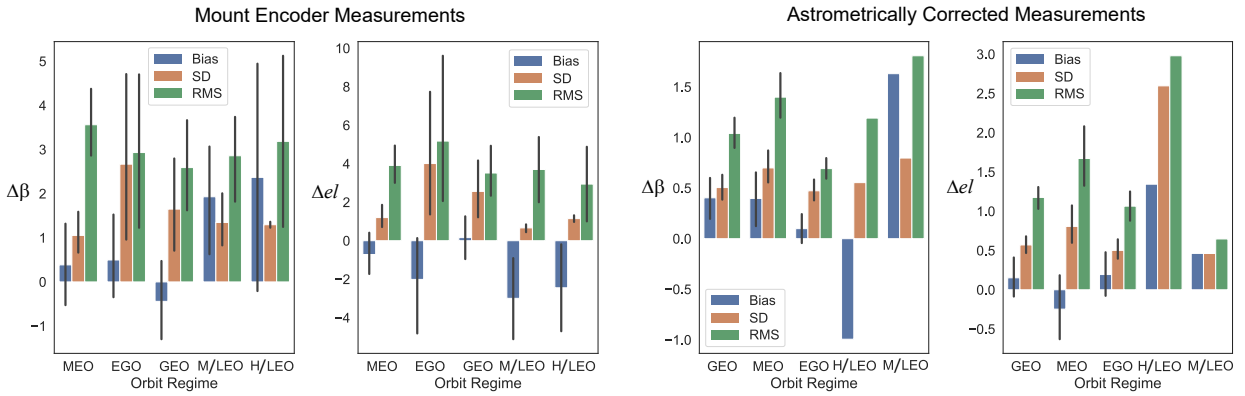

Figure 3. (a) Residuals between Correlated mount encoder measurements on all sensors at Learmonth compared to SERC/EOS OD ephemeris data. (b) Residuals between astrometrically corrected measurements for all Sensors at Learmonth compared to SERC/EOS OD ephemeris data

Next, we propagate the state generated by the OD process backwards and compare it with the observations before the OD span. If observations fall outside a predefined threshold which grows as a function of time, this is an indication that perhaps the propagated state and corresponding OD results need further investigation. In order to determine this threshold, historic data is fitted that resulted from orbit determinations that yielded practical ballistic and/or solar radiation coefficients, reasonable RMS residuals during the OD span and led to successfully aquiring objects in the narrow field of view of the telescope's camera. The procedure begins by taking each tracklet and placing into daily bins. The RMS of the residuals for each bin is then calculated. The reason for this is that we typically calculate the tracklet RMS to test against a threshold which changes with time. If an overall RMS of the residuals is calculated, then we will only have an average of the overall drift and we lose the concept of drift in the propagated state.

In order to demonstrate the results from this process, the tracklets from comparing astrometrically corrected observations to back propagated states from hundreds of OD processes were used that have been stored in the catalog. The type of objects considered are the same as above, i.e., non-operational and debris. In Fig. 4, these tracklets are placed in daily bins and the RMS values of each are calculated, which has been performed for several orbital regimes including High LEO, MEO, GEO and EGO. The orbits from GEO, EGO to MEO (Figs. 4(a),4(b),4(c)) only show about $2-3''$ drift after a week, which will easily land an object to within the narrow field of each telescope, giving sufficient accuracy for unaided acquisition for active laser ranging. In the case of High LEO targets in Fig 4(d) we see a larger drift, but only about $7''$ after 4 days which will still be sufficient for aquiring targets for laser ranging. In order to estimate the drift for automated purposes, a linear regression model can be fitted to the data as a function of days out from the OD span.

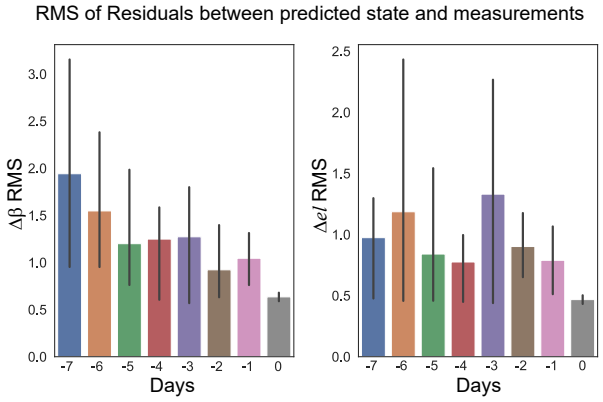

(a) GEO

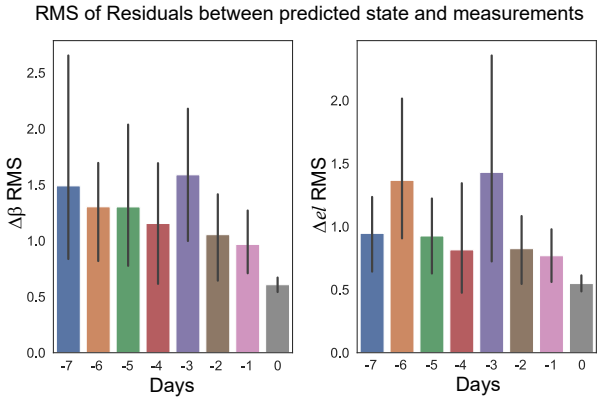

(b) EGO

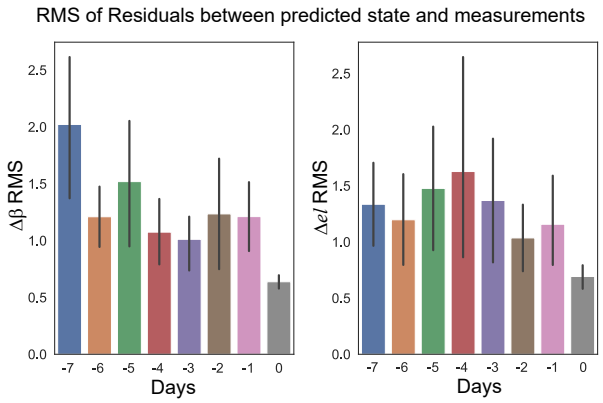

(c) MEO

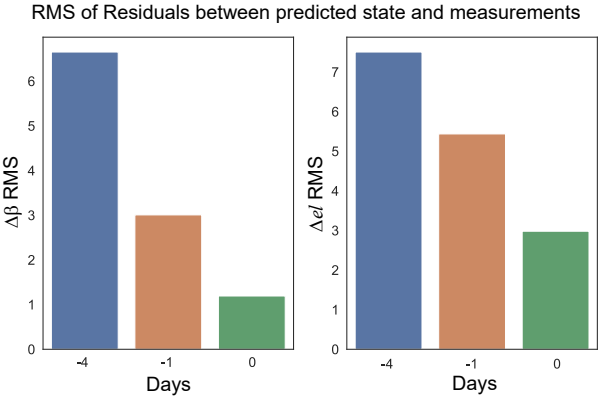

(d) High LEO

Figure 4

4. CONCLUSIONS

In this paper, we discussed a method to automatically maintain and build a new catalog of active/defunct space assets and debris. The procedure began by demonstrating how the force parameters are seeded before the OD process commences, which involved using coefficient from historic OD cases, or alternative approach when they are not available like the Ballistic Coefficient Estimation Method. An example of the level of sensor noise to tune the weighting for the OD process was demonstrated and then the bias, standard deviation and RMS of the residuals during the OD span was discussed. The next step then looked at the propagation error by comparing the back propagated state (transfered to observation space) against astrometrically corrected observations before the initial OD epoch. It was observed that the residuals for higher earth objects experienced a drift after a week of only a few arc-seconds; High LEO targets had a higher drift, while insufficient data was available during the recent campaign to assess lower LEO orbits. At the drift rates for higher orbits it is expected future propagations would land targets within the narrow field of view of all telescopes thus facilitating acquisition and sensor throughput.

Future implementations aim to automate the assessment of the consistency between ephemeris data generated from different OD processes which overlap or comparison to external reference orbits when available. In addition, we aim to incorporate a method which assesses whether the covariance from the batch-least squares process are too optimistic which can affect sensor throughput by erroneously rejecting observations during object correlation. Highly optimistic covariances can also yield incorrectly low collision probabilities.

ACKNOWLEDGEMENTS

The authors would like to acknowledge the support of the Cooperative Research Centre for Space Environment Management (SERC Limited) through the Australian Governments Cooperative Research Centre Programme. They would also like to take this opportunity to thank James Allworth and Zahra Carn for their assistance.

References

[1] V. O. Korkiakoski, J. D. Grosse, F. Bennet, and F. Rigaut. Single detector stereo-SCIDAR for Mount Stromlo: Data analysis', Laser Communication and Propagation through the Atmosphere and Oceans. *SPIE*, page 11, 2016.

[2] D. Kucharski1 and et. al. Photon Pressure Force on Space Debris TOPEX/Poseidon Measured by Satellite Laser Ranging. *Earth and Space Science*, 4:661–668, 2017.

[3] M. Möckel, J. Bennett, E. Stoll, and K. Zhang. High performance orbital propagation using a generic software architecture, September 20-23, 2016 2016.

[4] Sven Flegel, James Bennett, Michael Lachut, Marek Möckel, and Craig Smith. An analysis of the 2016 hitomi breakup event. *Earth, Planets and Space*, 69(1):51, 2017.

[5] J. Sang, J. C. Bennett, and C. H. Smith. Estimation of ballistic coefficients of low altitude debris objects from historical two line elements. *Adv. Space Res.*, 52(1):117–124, 2013. 10.1016/j.asr.2013.03.010.

[6] USC Satellite Database, 201. `http://www.ucsusa.org/nuclear-weapons/space-weapons/satellite-database.html#.VnC1HTgVhaS`.

[7] T. Flohrer and Frey. S. Classification of Geosynchronous Objects, 2016.

[8] D. A. Vallado. *Fundamentals of Astrondynamics and Applications*. Microcosm Press & Springer, CA & New York, 4th edition, 2013.